Journal Pre-proof

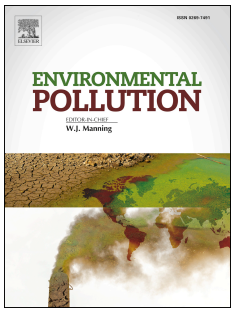

Vertical distribution of smoke aerosols over upper Indo-Gangetic Plain

Kameswara S. Vinjamuri, Alaa Mhawish, Tirthankar Banerjee, Meytar Sorek-Hamer, David M. Broday, Rajesh K. Mall, Mohd Talib Latif

PII: S0269-7491(19)33052-0

DOI: https://doi.org/10.1016/j.envpol.2019.113377

Reference: ENPO 113377

To appear in: *Environmental Pollution*

Received Date: 10 June 2019

Revised Date: 5 August 2019

Accepted Date: 9 October 2019

Please cite this article as: Vinjamuri, K.S., Mhawish, A., Banerjee, T., Sorek-Hamer, M., Broday, D.M., Mall, R.K., Latif, M.T., Vertical distribution of smoke aerosols over upper Indo-Gangetic Plain, *Environmental Pollution* (2019), doi: https://doi.org/10.1016/j.envpol.2019.113377.

Graphical abstract

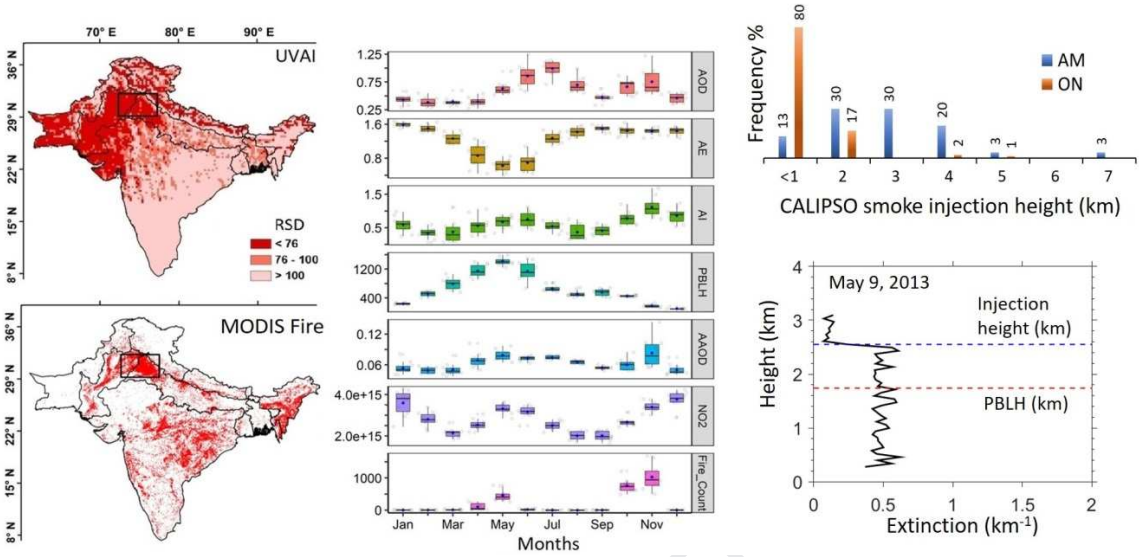

Variations of OMI UVAI and MODIS fire count with smoke injection height against the PBLH.

Vertical distribution of smoke aerosols over upper Indo-Gangetic Plain

Kameswara S. Vinjamuri[1], Alaa Mhawish[2], Tirthankar Banerjee[1,2*], Meytar Sorek-Hamer[3], David M. Broday[4], Rajesh K. Mall[1,2] and Mohd Talib Latif[5]

[1]DST-Mahamana Centre of Excellence in Climate Change Research, Banaras Hindu University, Varanasi, India.
[2]Institute of Environment and Sustainable Development, Banaras Hindu University, Varanasi, India.
[3]NASA Ames Research Center, Moffett Field, CA, USA.
[4]Civil and Environmental Engineering, Technion, Hafia, Israel.
[5]Center for Earth Sciences and Environment, Faculty of Science and Technology, Universiti Kebangsaan Malaysia, Bangi, Malaysia.
**Correspondence to*: T. Banerjee (tb.iesd@bhu.ac.in; tirthankaronline@gmail.com)

Abstract

Attenuated backscatter profiles retrieved by the space borne active lidar CALIOP on-board CALIPSO satellite were used to measure the vertical distribution of smoke aerosols and to compare it against the ECMWF planetary boundary layer height (PBLH) over the smoke dominated region of Indo-Gangetic Plain (IGP), South Asia. Initially, the relative abundance of smoke aerosols was investigated considering multiple satellite retrieved aerosol optical properties. Only the upper IGP was selectively considered for CALIPSO retrieval based on prevalence of smoke aerosols. Smoke extinction was found to contribute 2-50% of the total aerosol extinction, with strong seasonal and altitudinal attributes. During winter (DJF), smoke aerosols contribute almost 50% of total aerosol extinction only near to the surface while in post-monsoon (ON) and monsoon (JJAS), relative contribution of smoke aerosols to total extinction was highest at about 8km height. There was strong diurnal variation in smoke extinction, evident throughout the year, with frequent abundance of smoke particles at lower height (<4km) during daytime compared to higher height during night (>4km). Smoke injection height also varied considerably during rice (ON: 0.71±0.65km) and wheat (AM: 2.34±1.34km) residue burning period having a significant positive correlation with prevailing PBLH. Partitioning smoke AOD against PBLH into the free troposphere (FT) and boundary layer (BL) yield interesting results. BL contribute 36% (16%) of smoke AOD during daytime (nighttime) and the BL-FT distinction increased particularly at night. There was evidence that despite travelling efficiently to FT, major proportion of smoke AOD (50-80%) continue to remain close to the surface (<3km) thereby, may have greater implications on regional climate, air quality, smoke transport and AOD-particulate modelling.

Keywords: Aerosol; Boundary layer; CALIPSO; Geospatial analysis; Smoke.

Capsule: Smoke aerosols were most abundant over upper Indo-Gangetic Plain and 50-80% of smoke AOD remain close (< 3 km) to the surface.

1. Introduction

Smoke particles are carbonaceous aerosols emitted primarily from the burning of biomass and fossil fuels (e.g., oil, petroleum, natural gas, coal). Incomplete combustion of fossil fuel results in emissions of black carbon aerosols which absorbs solar radiation at the visible and near-IR (NIR) ranges (Andreae and Gelencser, 2006; Eck et al., 2013). In contrast, the open/ indoor biomass combustion for residential cooking and heating emits black carbon, brown carbon and different organic aerosols (Chung et al., 2012; Kirchstetter et al., 2004). Here, the portion of carbonaceous aerosols that typically absorbs insolation at the UV-Vis-NIR is referred as smoke particles (Eck et al., 2013; de Vries et al., 2013). To define optically, we followed the classification given by Kim et al. (2018) which explain the smoke aerosol based on no/-minimum depolarization with lidar ratios of 70 sr at 532 nm and 30 sr at 1064 nm. Due to their atmospheric abundance and light-absorbing properties, smoke aerosols influence climate by means of changing thermal structure of the atmosphere (Wang, 2004), promote vertical stratification both in the free troposphere (FT) and within the boundary layer (BL) (Babu et al., 2011), and induce large-scale modulations to atmospheric circulation processes (Lee and Kim, 2010). Beside these, interactions between smoke aerosols and cloud droplets can modify cloud formation (Koren et al., 2004), increase dissipation (Bond et al., 2013) and may also reduce precipitation (Feingold et al., 2001). Smoke aerosols also vowed to be toxic in nature thereby, pose greater potential to impact human health (Janseen et al., 2011, Ho et al., 2018).

The Indo-Gangetic Plain (IGP), South Asia, is one of the global aerosol hotspot, documented extensively to experience the highest (Kumar et al., 2018a; Singh et al., 2017a; Sen et al., 2017; Dey and Di Girolamo, 2011) and most diverse burden of aerosol loading (Gautam et al., 2010, 2011; Mhawish et al., 2017; Dey et al., 2004), with considerable spatio-temporal variations in aerosol types and properties (Jethva et al., 2005; Singh et al., 2017b; Sayer et al., 2014; Mhawish et al., 2018). Second only to vehicular emissions, biomass burning emissions are the principal sources of smoke aerosols across the IGP (Singh et al., 2017a). In particular, the post-harvest specific agricultural residues burning emits huge amount of smoke aerosols (Rajput et al., 2014; Singh et al., 2017b, 2018; Vadrevu et al., 2011), which frequently transport down-wind and deteriorate ambient air quality in the cities like Delhi (Jethva et al., 2018; Chowdhury et al., 2019) and Varanasi (Singh et al., 2018). Additional sources of smoke aerosols often have episodic nature, e.g. lighting fire crackers during festive season (Kumar et al., 2016) or backyard incineration of waste material (Banerjee et al., 2017; Sharma et al., 2019). The elevation at which the smoke aerosols used to inject into the atmosphere is critical as it strongly regulate its subsequent transport, atmospheric chemistry, dilution and climatic implications (Amiridis et al., 2010; Guan et al., 2010; Bourgeois et al., 2018;

Kahn et al., 2008). Besides, on the radiative forcing aspect, the information of smoke aerosol layer height is crucial as durng long-range transport it may frequently overlie low-level clouds resulting in aerosol-cloud overlap (Meyer et al. 2015; Jethva et al., 2018), leading to positive radiative forcing and atmospheric warming (Zhang et al., 2016). Defined as the altitude at which smoke particles are first introduced to the atmosphere before transport (Kahn et al., 2008); only few research groups have attempted to effectively measure the smoke injection height by means of using space-borne lidar (Bourgeois et al., 2018; Amiridis et al., 2010; Labonne et al., 2007; Mims et al., 2010), considering stereo-derived plume heights (Kahn et al. 2008; Chen et al., 2009) or by using proxies like aerosol index (Guan et al., 2010). In majority of the cases, the approach was to parameterize the smoke extinction against the planetary boundary layer height (PBLH) which effectively relate smoke chemistry and transport processes. Typically, within the PBLH (BL), the atmosphere is well-mixed with more efficient removal processes compared to the free troposphere (above PBLH, FT) where aerosols are less subject to atmospheric reactions, resulting into greater residence time, leading to possibilities for long-range transport (Stull et al., 1988; Bourgeois et al., 2018). Effective parameterization of the smoke injection height in regional air quality/-climate model, and to recognize vertical stratification of smoke aerosol in terms of BL and FT are therefore, crucial to reciprocate chemical reactivity of smoke aerosols, its residence time, long-range transport, radiative forcing and for estimating surface-level exposure.

Beside characterization of optical and physical properties of smoke aerosols, considerable uncertainties still exist in vertical distribution of smoke aerosols and smoke injection height across South Asia. Although few attempts were made in global (Bourgeois et al., 2018; Koffi et al., 2016; Toth et al., 2016) and regional perspectives (Chen et al., 2009; Amiridis et al., 2010; Guan et al., 2010; Val Martin et al., 2009; Labonne et al., 2007), across India the approaches were mainly isolated over certain region and dedicated chiefly for episode specific analysis (Satheesh et al., 2009; Babu et al., 2011). This instigate us to make use of attenuated backscatter profiles from the CALIOP (Cloud-Aerosol Lidar with Orthogonal Polarization; Winker et al., 2009, 2013; Young and Vaughan, 2009) sensor over the smoke dominated region of South Asia to characterize vertical profile of smoke aerosols and to explore its geometrical properties. To our knowledge, this would be the first of its kind long-term observation of smoke aerosol over South Asia with smoke aerosols partitioned against the boundary layer. However, beside exploring the entire geographical region of South Asia, we took few proxies for geospatial analysis of aerosols for identifying the area with maximum dominance of smoke particles, and further evaluated the nature of smoke distribution under different time scale. Our analysis has implications to the air quality/ climate modellers in particular

and have also applications in regional columnar aerosol-particulate modelling, aerosol transport and in epidemiological research.

2. Experimental methods

2.1 Satellite-based observations

2.1.1 Aqua/-Terra MODIS data

Moderate Resolution Imaging Spectroradiometer (MODIS) on board the EOS Terra (from 2000) and the Aqua (from 2002) satellites measures the earth and atmospheric radiance, and provide images in 36 spectral bands between 0.415 and 14.235 μm, with spatial resolution varying from 250 m to 1 km (Levy et al., 2013; Mhawish et al., 2017; 2019). The MODIS wide swath (~2330 km), with global coverage in every 1-2 days, permits consistent monitoring of the earth land surface and atmosphere. Many algorithms have been used to process the measured MODIS radiance at different bands for retrieving aerosols (Levy et al., 2013; Lyapustin et al., 2018, Bilal et al., 2014), fire characteristics (Giglio et al., 2003), and land surface coverage (Lyapustin et al., 2012, Vermote and Kotchenova, 2008). In this work, the latest version of Aqua MODIS (C6.1) aerosol products (i.e. aerosol optical depth, AOD, and Angstrom exponent, AE) retrieved using enhanced Deep Blue (DB) algorithm, and the Aqua & Terra C6 MODIS fire products (i.e. active fire count) have been used for estimating aerosol loading, aerosol types and biomass burning, respectively.

MODIS AOD retrievals by different algorithms have been widely validated and used both on global (Gupta et al., 2018; Wei et al., 2019; Sayer et al., 2019) and at regional basis (Mhawish et al., 2017, 2019; Kumar et al., 2018a; Bilal and Nichol, 2015). Here we used Aqua MODIS C6.1 DB aerosol data products considering its capability of retrieving aerosols over varied land surfaces (from arid to dark vegetated surfaces) except over snow and ice. Against ground-based sun-photometer Aerosol Robotic Network AOD (AERONET), the latest MODIS C6.1 DB AOD provide better agreement compared to the previous C6 version (Sayer et al., 2019; Wei et al., 2019), which we earlier reported to underestimate AOD across the IGP (Sayer et al., 2014; Mhawish et al., 2017). The highest quality (QA>2) DB AOD from 2008 to 2017 (all inclusive) was therefore, used to examine the temporal variations of aerosol loading over the study region. Additionally, DB AE with recommended quality flag (QA>2) was also used as a qualitative parameter to classify the aerosol types into coarse mode (AE<0.7), mixed mode (0.70<AE<1.25), and fine mode (AE>1.25) aerosols (Sayer et al., 2014).

Aqua and Terra MODIS C6 Level 2 fire products (confidence > 80%), including actively burning fire (fire count), have been retrieved from Fire Information for Resource Management System (FIRMS, https: //firms.modaps.eosdis.nasa.gov). The spatial resolution of the MODIS fire

products is 1 km at nadir, increasing up to 4.8 km at the edge of the scan. Considering strong mid-infrared radiation from active fire, MODIS detects fire based on brightness temperature using both the 4 µm and 11 µm bands (Gilio et al., 2003). MODIS fire products from both Aqua and Terra were retrieved on a daily basis and were averaged for similar timeframe (2008 to 2017, inclusive).

2.1.2 Aura-OMI data

OMI is a hyper-spectral imaging spectrometer aboard A-train's Aura satellite (sun-synchronous), and is instrumental in measuring solar backscatter irradiation at the top-of-the-atmosphere (TOA) in UV–visible spectrum range (264-504 nm; Levelt et al., 2006). The capability of measuring near-UV aerosol properties enables OMI to provide UV-Aerosol Index (UVAI), which has been widely used to project global/-regional distribution of UV-absorbing aerosols like carbonaceous aerosols, desert dusts and volcanic ash (Herman et al., 1997; Torres et al., 2007; Zhang et al., 2017; Singh et al., 2018; Jethva et al., 2018). The UVAI is a semi-quantitative parameter, and a function of the AOD, the aerosol absorption and the aerosol layer height. OMI Near-UV aerosol retrieval algorithm (OMAERUV) uses 354 nm and 388 nm spectral measurements to compute UVAI using the following equation (Torres et al., 2007):

$$UVAI = -100\ log_{10}\left(\frac{I^{m}_{354}}{I^{c}_{354}R^{*}_{354}}\right)$$

where I^{m}_{354} is the TOA radiance measured by the OMI and I^{c}_{354} is the calculated radiance for a pure Rayleigh scattering atmosphere with a Lambertian surface reflectance of R^{*}_{354} at 354 nm. UVAI is useful to provide information on aerosol UV absorption when used in combination with AOD (de Vries et al., 2015; Torres et al., 2007, 2013). Here, UVAI is retrieved from Level-2 collection 003 (V1.4.2) daily grid data (OMIL2G) at 0.25° x 0.25° resolution and averaged spatially. Recent upgrades and uncertainty related to the retrieval of UVAI by OMAERUV are explained in Torres et al. (2013). The OMI absorbing aerosol optical depth (AAOD) was retrieved from gridded level 2 (L2G) AAOD at 388nm (V1.4.2) with 0.25-dgree spatial resolution for 10 years (2008 to 2017). Only the AAOD retrievals associated with quality flag "1" was consider for this analysis.

Besides UVAI and AAOD, we have also considered collocated measurements of trace gases (like NO_2) to ascertain the main sources of biomass burning aerosols. As reported by Veefkind et al. (2011), presence of significant correlation between AOD and NO_2 indicate possible sources of aerosol. Therefore, tropospheric NO_2 column density was retrieved from Aura-OMI Level 3 version 003 daily 0.25° x 0.25° gridded OMNO2d product (cloud fraction <30%; Krotkov et al., 2017).

2.1.3 CALIPSO-CALIOP observations

The CALIOP (Cloud-Aerosol Lidar with Orthogonal Polarization) sensor on board the polar orbiter Cloud-Aerosol Lidar and Infrared Pathfinder Satellite Observation (CALIPSO) is a two-wavelength elastic polarization lidar (532 nm and 1064 nm) that measures attenuated backscatter radiation and provides globally the vertical distribution of cloud, aerosols, aerosol layer height and aerosol types (Winker et al., 2009). The CALIOP retrieves aerosol profiles at various vertical resolutions like in 30 m (surface to 8.2 km) and in 60 m (from 8.2 to 20.2 km). The detailed information about the CALIPSO aerosol retrieval algorithm is included in Winker et al. (2009), Kim et al. (2018) and in Young and Vaughan (2009). CALIOP has a better signal-to-noise ratio and aerosol extinction detection sensitivity at night due to the absence of solar background illumination. It has an overall aerosol detection sensitivity of 0.01 to 0.07 km^{-1}, having potential underestimation of low aerosol extinction at high altitudes and in the FT (Winker et al., 2013; Toth et al., 2018). Besides, during heavy smoke aerosol loading condition, CALIOP lidar at 532 nm often attenuates quickly resulting miss approximation of aerosol layer height which also result into underestimation of AOD (Torres et al., 2013; Jethva et al., 2014). The CALIOP V4 AOD has been validated both globally (Kim et al., 2018) and regionally (Kumar et al., 2018b; Bourgeois et al., 2018) against AERONET/ MODIS observation. Over South Asia, CALIOP AOD is reported to have better agreement with AERONET (Kim et al., 2018). At a high-altitude site in the Himalayas, CALIOP recorded 87% AOD retrieval within the expected error (Kumar et al., 2018b). However, there are cases when CALIOP AOD is reported to underestimate AOD, especially at free troposphere with low aerosol extinction coefficient (Bourgeois et al., 2018).

Here, 10-years (2008 to 2017) of aerosol extinction coefficients were extracted from the latest and improved CALIOP version 4.10 (V4) Level 2 5-km aerosol profiles. CALIOP V4 Level 2 adopted many upgrades from the previous versions to reduce uncertainties, especially in terms of retrieving stratospheric aerosols and revising lidar ratio for few aerosol subtypes. This has led to improve retrieval of mean AOD at 532 nm by 40-52% (Kim et al., 2018). To retrieve smoke aerosols, we considered two aerosol sub-types i.e. polluted continental/smoke and elevated smoke, retrieved based on the criteria given by Kim et al. (2018) and Bourgeois et al. (2018). In CALIOP V4, lidar ratio at 532 nm for polluted continental/smoke remain identical as in version 3 (70 ± 25 sr), but lidar ratio was upgraded with better sensitivity for elevated smoke from 70 ± 28 sr to 70 ± 16 sr. Further, only non-negative aerosol extinctions, with extinction quality flags of 0, 1, 18 or 16 that meet the cloud-aerosol discrimination (CAD) criterions (CAD≤-20; ≠ -101) were used to retrieve AOD.

2.2 ERA-Interim data

The planetary boundary layer height (PBLH) was obtained from the European Centre for Medium-range Weather Forecasts (ECMWF) Re-Analysis-Interim (ERA-Interim) dataset. The ECMWF PBLH is based on data assimilation from different earth observation satellites and numerical weather prediction models, and has higher spatial and temporal resolution compared to other reanalysis data (such as MERRA 2, GDAS). It is also reported to have better agreement with PBLH obtained by other methods (von Engeln and Teixeira, 2013). The PBLH was retrieved at 0.125˚ X 0.125˚ horizontal resolution and at 3-h temporal resolution (11:38:50 UTC to 14:38:50 UTC), and was spatially averaged in order to match the CALIPSO overpassing time.

2.3 Data processing

We have employed multiple datasets consisting both aerosol optical (AAOD, AOD, UVAI) and microphysical properties (AE) retrieved over a span of 10 years (2008-2017) to ascertain spatio-temporal variation of aerosols. UVAI is a widely used parameter for absorbing (+ve UVAI) and scattering (-ve UVAI) aerosols (Torres et al., 2013; Singh et al., 2018; Jethva et al., 2018) while AE is used to classify aerosol according to its size (Mhawish et al., 2017; 2019; Sayer et al., 2014). Initially, the spatial distribution of the columnar aerosol loading, aerosol type and the distribution of absorbing aerosols over South Asia were explored, to identify the region(s) with consistent dominance of fine and absorbing aerosols. Further, the absorbing aerosol source region was assessed by geospatial analysis considering few proxies of smoke aerosols like prevalence of high (+) UVAI, high AAOD, high UVAI relative standard deviation (RSD) with corresponding high AOD (indicating high aerosol loading) and high AE (suggesting dominance of finer particles). After identifying the region with maximum dominance of smoke aerosols, observational evidences regarding the aerosol properties were explored, emphasizing the kind of aerosols persisting over the region and their spatial and vertical distribution. Prevailing aerosols were classified into nine aerosol types (de Vries et al., 2015), considering AE as a proxy of the aerosol size (coarse, AE<0.7); mixed, 0.7<AE<1.2; fine, AE>1.2) and UVAI as aerosol type (scattering, UVAI<0.0; absorbing, UVAI>0.00). Only the mean values of the highest quality pixels of the UVAI and AE over the study area were used to classify aerosol types.

To investigate the vertical distribution of aerosol, CALIOP vertical profiles that fall within the selected box have only been analysed. A total of 82,156 CALIOP 5 km vertical profiles from 594 (810) CALIPSO paths were processed to retrieve smoke AOD, 48% (52%) of which were retrieved during daytime (nighttime). CALIPSO smoke injection height was calculated based on the gradient method which consider the particular height at which the minimum extinction coefficient was retrieved after a steep decrease in the attenuated backscatter (Menut et al., 1999; Amiridis et al., 2010). However, it is noteworthy that the smoke injection height measured here is a representative of the selected

region as we used Level 2 dataset that have fixed spatial resolution of 5 km. However, no significant variation in the shape of the aerosol layer was earlier reported between 5-km Level 2 CALIPSO product against 1-km horizontally averaged CALIPSO profiles (Amiridis et al., 2010). Moreover, as the ECMWF reports PBLH corresponds to height above the topographical surface whereas CALIPSO considers mean sea level as its reference point, we also made the necessary correction to ECMWF PBLH dataset to make both in a same reference scale.

Here, CALIOP AOD is computed from the CALIOP aerosol extinction profiles following Bourgeois et al. (2018). Smoke aerosol vertical distribution with respect to PBLH were examined in terms of smoke optical depth within the PBLH (boundary layer, BL) and within the free troposphere (FT). ERA-Interim PBLH were used to segregate the AOD within and above the boundary layer. To match the temporal resolution of CALIOP with PBLH, two closest time steps of ERA-Interim data with CALIOP overpass time were averaged. To constitute the relative contribution of smoke aerosol against total aerosol loading (as in section 3.3), we compared the extinction coefficient of smoke aerosols to the total extinction retrieved at each vertical bin. Cases in which no smoke aerosols were retrieved were marked by 0, denoting a null contribution of smoke to the total aerosol extinction. In the following sections 3.4 and 3.6, only bins in which smoke was detected were considered.

3. Results and discussion

3.1 Spatial variability of aerosols

Figure 1 denotes climatological distribution of aerosol loading, absorbing aerosols and the size of the aerosols over South Asia, averaged over the period of 2008 to 2017. Invariably, presence of high aerosol loading (AOD>0.45) was evident only over the IGP (Fig. 1a), in comparison to South Asia which otherwise exhibit comparatively low AOD. Indeed, in the last decade the area-weighted mean (±SD) AOD over the IGP was 0.55 (±0.21) compared to 0.31 (±0.21) over the rest of South Asia. The inter-annual variability of AOD was about 7%, noted most strongly over the central IGP (see also Kumar et al., 2018a). A strong seasonality in aerosol loading was retrieved across IGP, with ON (post-monsoon; AOD, mean±SD: 0.54±0.20) and DJF (winter; 0.48±0.18) remained the most polluted seasons. In contrast, the high AOD retrieved during JJAS (monsoon; 0.57±0.16; Fig. 1) refer the moisture induced hygroscopic growth of hydrophilic aerosol particles (Altaratz et al., 2013). The spatial variation of absorbing/ scattering aerosols across South Asia (Fig. 1b) depicts the presence of scattering aerosols over the northern and north-eastern parts of India, coinciding with the foothills of the Himalaya. In contrast, there was clear dominance of absorbing aerosols over the western dry regions and over the Gangetic plain. A very high UVAI (>0.75) was however, only retrieved over the northwestern dry regions, Indian states of Punjab, Haryana, western Uttar Pradesh, and in the

Punjab state of Pakistan; the region often reported to be responsible for large emissions of carbonaceous aerosols from burning of agricultural residues and fossil fuels (Singh et al., 2018; Rajput and Sarin, 2014; Jethva et al., 2018). The IGP also experienced very high inter-annual (~20%) and intra-seasonal variations in UVAI with the highest UVAI during ON (mean±SD: 0.61±0.27) and the lowest during MAM (0.53±0.23). The spatial variation of the absorbing aerosol optical depth (AAOD), a reliable quantitative aerosol product that is recognized as a direct proxy of absorbing aerosol (black carbon, light-absorbing organic carbon, and desert dust; Zhang et al., 2015, 2016) was evident as high over the northwestern dry region, extended to the parts of central IGP. To ascertain the relative size of airborne particles, 10-years average MODIS AE was included for comparison. There was complete dominance of fine aerosols across South Asia except for the northwestern dry part where mixed aerosols prevailed. Beside these, strong seasonal variations are also noticed, with fine particles completely engulfing South Asia during ON and DJF while coarse and mixed-size aerosols prevailing during MAM and JJAS, particularly over the northwest and central highlands.

Overall, the presence of highly absorbing fine particles over the upper IGP during ON and DJF indicates the abundance of carbonaceous aerosols (like smoke), emitted from the burning of bio/-crop residues and fossil fuels (Singh et al., 2018; Jethva et al., 2018). In contrast, the less absorbing coarse-to-mixed aerosols observed during MAM and JJAS over central and lower IGP probably indicate occasional mixing of locally emitted pollutants with crustal materials and desert dust, often of transboundary origin (Kumar et al., 2018a; Sen et al., 2017; Dey et al., 2004; Gautam et al., 2010; 2011). To further ascertain the source region of highly absorbing fine particles, we analysed 10 years of the UVAI relative standard deviation (RSD) over South Asia. Very high UVAI RSD (coefficient of variation, CoF>75) was noted across the South Asia (Fig. 2), except over the north-western dry parts. However, only over the upper IGP (72.40 W, 32.25 N, 77.22 E, 29.30 S) it follows the spatial pattern of very high UVAI, AAOD, AOD and high AE. We considered all these evidences as the proxy of smoke aerosols and therefore, only prioritized on retrieving and analysing vertical profiles of smoke aerosols over the selected region.

3.2 Temporal variability of aerosols over the upper IGP: Constraining aerosol type

Figure 2 illustrates the temporal variation of different aerosol parameters over the selected box derived from a 10-year's record of OMI & MODIS measurement, with descriptive statistics included in Table S1 and S2. The spatial variation of UVAI RSD (Fig. 2a) and MODIS fire count (Fig. 2b) represent annual mean while Fig. 2c indicates monthly means based on decadal dataset. Here, we wished to make most realistic estimate of existing aerosol type considering satellite retrieved aerosol optical properties (e.g. AE and UVAI) and emission of trace gases as a proxy for aerosol precursors.

Over the box, AOD was particularly high during JJAS (mean±SD: 0.84±0.35; range: 0.6-1.0), especially in June and July (AOD>0.84). Such high AOD is due to the result of available moisture present during onset of monsoon. AOD declined gradually during August-September together with an increase in AE (>1.3), possibly due to partial removal of coarse aerosols by monsoon rain. The distinction of prevailing aerosol type was critical as it could be affected by the invasion of sea salt aerosols (large, non-absorbing) mixed with smoke aerosols (small, absorbing), with additional contribution from desert dusts (large, absorbing) and industrial pollution (small, mild-absorbing). Besides monsoon, the AOD remains high particularly during October to December (OND; mean±SD: 0.63±0.40) with clear dominance of fine (AE: 1.43±0.25) and absorbing aerosols (UVAI: 1.04±1.55). Presence of highly absorbing aerosols with small particle size during OND indicates smoke aerosols. UV absorbing fine particles continue to dominate aerosol loading till January, before reducing to the lowest in early summer (February-March). During early summer, both AOD (0.40) and UVAI (0.34-0.39) remain low along with high AE (1.26-1.50) refer the mixing of small absorbing aerosols (smoke) with neutral-to-less absorbing fine particulates (like secondary organic/ biogenic aerosols, secondary aerosols of industrial/ urban source), along with a small fraction of desert dust. During summer, a consistent increase in UV-absorbing aerosols from April (UVAI: 0.56) to June (UVAI: 0.76) and a corresponding increase in the AOD (from 0.40 to 0.84), together with a decrease in the AE (0.86 to 0.63) possibly indicates mixing of smoke aerosols with mineral dusts and other anthropogenic aerosols.

We attempted to classify the existing aerosol type following de Vries et al. (2015) aerosol classification scheme. For the 10-years MODIS-OMI collocated observations (3270), smoke aerosol was found to dominate 41% of the days, which increased up to 67% from October to February. We also took MODIS fire count and OMI-NO_2 concentration as a proxy for emission of aerosols and its precursors. Two distinct peaks in the MODIS fire count and in the OMI-NO_2 concentrations ($x10^{15}$ molecules cm^{-2}) were observed, one in April-May (monthly mean fire count: 104-460; NO_2: 3.23±0.71) during wheat resides burning and one in October-November (759-1030; 3.24±1.17), coinciding well with the rice residues burning period. The highly significant correlation between the AOD with fire count and NO_2 concentrations also provides direct observational evidence of biomass burning emissions and smoke aerosols prevalence over the upper IGP, having potential direct consequence on the regional radiative budget, cloud microphysical properties and on human health.

3.3 Vertical distribution of smoke aerosols

The CALIPSO aerosol profiles over the selected region of upper IGP were processed assuming negligible spatial variations in the aerosol types. To retrieve CALIPSO smoke aerosols, both polluted continental/smoke and elevated smoke aerosol types were considered and was compared

against total aerosol extinction. Figure 3 depicts the seasonal variations in the smoke aerosol extinction against total aerosol (Fig. 3a-d), the annual trend (Fig. 3e), and the altitudinal distribution of the relative contribution of smoke to total aerosol extinction (Fig. 3f). In every case, the maximum extinction of total/-smoke aerosols appeared to be at the surface, although with varying coefficient, before reducing with the increasing height. Only conflict to this general observation was during JJAS for smoke aerosols with slight increase in extinction against the surface, but was not explored further. Overall, near surface total aerosol extinction remain >0.1 km^{-1} throughout the year with smoke contribution varying from ~ 2 to 50%. The smoke extinction decreased gradually up to a height of 4 km before reaching to a zone of accumulation at about 6 to 8 km. Presence of smoke at a high altitude across the seasons indicate the possible contribution of transboundary aerosols and/-or convective transfer of smoke aerosols from the surface, whichever the case may be. There was a signature of total aerosols extended till a height of 14 km or beyond, almost 1.5 times higher against smoke aerosols. This was more prominent during MAM and JJAS when the PBLH was maximal.

Among the seasons, the near-surface smoke extinction was highest during DJF, contributing up to 50% of total aerosol extinction and minimum during MAM and JJAS (~ 2-5%). The small relative contribution of smoke to the near surface total extinction during MAM and JJAS mainly results from the crucial influence of crustal/ desert dusts to the total aerosol and deeper boundary layer due to convective mixing. Relative contribution of smoke to total aerosols also varied vertically with an increase in smoke percentage from 5.5 to 8.0 km for all the seasons except MAM. This was particularly evident during ON and JJAS when smoke aerosol contributed up to 50% of total extinction at 8 km while during DJF, the corresponding peak was at 6 km height. However, it should be noted that the contribution of smoke aerosols to total aerosol extinction is presented in relative term as aerosol concentration generally increases near ground compared to the higher altitude. The heterogeneity in smoke aerosols with height may have significant implications on aerosol transport and on regional climate, therefore was analysed against PBLH under day and night scenarios.

3.4 Diurnal variation of smoke extinction against PBLH

The diurnal variations of smoke aerosol extinction and day/-night occurrence frequency are depicted in Fig. 4 and 5. Clearly the nighttime smoke extinction remained high and elevated compared to the daytime. Daytime underestimation of aerosol extinction by CALIOP may also be influenced by the solar background illumination which often affect daytime feature detection of weakly scattering aerosols. The vertical distribution of aerosols during DJF indicates the persistence of smoke both within the FT and BL. During daytime, smoke profile reduced gradually with increasing height before accumulating at 3 km although with much lower intensity (0.3 km^{-1}) compared to the surface (1.2 km^{-1}). The day minus night (DN; Fig. 5) aerosol occurrence frequency

refer the nighttime presence of smoke aerosols more frequently at FT (>4 km). A similar smoke profile was also noted during ON except with higher extinction possibly influenced by the biomass burning emissions near the surface. The maximum extinction (2-3 km^{-1}) was however, remained well within the BL before diminishing with the increasing height. During ON, the smoke diurnal profile remained identical except the height. At night, top layer height of the smoke (~ 7.2 km) was two times higher compared to daytime (~ 3.5 km) that too with reduced intensity, refer the strong influence of boundary layer dynamics in efficient mixing of aerosols. The DN occurrence frequency (Fig. 5) suggest more frequent daytime appearance of smoke aerosols within the lower atmosphere (<4 km) while at night, CALIPSO retrieved smoke aerosols more frequently at higher altitude (> 4 km). Overall, the vertical profile of smoke aerosols during two most intense biomass burning seasons (MAM and ON) indicate nighttime accumulation of smoke aerosols at relatively high altitude which was later found to dissipate, possibly driven by advective wind circulation.

During MAM, the most prominent feature of aerosol vertical profile was the accumulation of aerosols at a relatively high altitude (3-4 km), which was later found to enhance during night with peak smoke extinction almost comparable to the surface (1 km^{-1}). Retrieving elevated extinction at 3-4 km possibly indicate the accumulation of transboundary aerosols, consistently during nighttime which otherwise get dissipate due to convective mixing of aerosols. There are reports of high-altitude accumulation of dust particles over upper IGP during MAM (Gautam et al., 2010), which subsequently mix with local/ regional smoke aerosols that are lifted to a higher altitude due to the influence of strong convective wind. Besides, this may also due to low daytime CALIOP signal-to-noise ratio which potentially affect the detection of weakly scattering aerosols, resulting into daytime underestimation of aerosol extinction. Vertical extinction of smoke aerosols during JJAS was similar to ON profile, although with much reduced intensity, before reducing monotonically with increasing height. The DN occurrence frequency of smoke aerosols during MAM and JJAS remain neutral till 6 km with equal probability of identifying smoke aerosols both during day and night.

3.5 CALIPSO retrieval of smoke injection height

The smoke aerosol injection height during burning of biomass/ agricultural residues across the upper IGP was examined using 10 years CALIPSO attenuated backscatter profile and was later compared against the prevailing ECMWF boundary layer height. Following the discussion in section 3.2, we note exclusive evidence of smoke aerosols emissions during AM (April-May, wheat residue burning) and ON (October-November, rice residue burning) and therefore, only these two seasons were considered for processing smoke injection height.

Two typical examples of CALIPSO V4 Level 2 attenuated backscatter coefficient and their corresponding first derivatives are included in Fig. 6, one at May 9, 2013 during wheat residue burning emission (Fig. 6a) and another at November 5, 2017 following rice residue burning emissions (Fig. 6b). Following the slope, the minimum derivative was found at 2.55 km in Fig. 6a compared to 1.18 km in Fig. 6b, representing the individual injection height of the smoke aerosols. Injection heights remain well above the PBLH in Fig. 6a while in Fig. 6b, the height remain relatively close to the PBLH. Overall, there was strong variation in mean smoke injection height between AM and ON possibly due to the varying influence of PBLH and fire activity at the surface. Likewise, during AM the smoke injection height varied between 0.34 km and 6.38 km a.s.l. with a seasonal mean (±SD) of 2.34 (±1.34) km. In contrast, the mean injection height (0.71±0.65 km) remained much closer to the surface during ON with a range between 0.28 and 4.25 km. Frequency distributions of the smoke injection height binned at 1 km height intervals is also included in Fig. 6e. During AM, 80% of injected smoke heights were retrieved between 1 and 4 km, while 97% of injection heights during ON were < 2 km. This clearly indicate that the average heights at which smoke aerosols injected into the atmosphere were much higher during wheat residue burning (in AM) compared to the rice residue burning period (in ON).

We also explored the CALIPSO smoke injection height against the ECMWF PBLH. In both the cases significant ($p<0.05$) positive association was noted with correlation coefficients varying from 0.26 (ON) to 0.38 (AM). The strong convective mixing during AM influences the PBLH and thereby, vertical movement of smoke aerosols. This possibly resulted in to 77% of the cases during AM when smoke was found to be injected directly at FT. In contrast, convective heat transfer from surface to atmosphere is low during ON, resulting in to low PBLH. This corresponded to 60% of smoke injection height remain below the PBLH. However, a low coefficient between injection height and boundary layer may be due to the fire radiative strength at the surface (Vadrevu et al., 2011), and due to the change in PBLH by strong thermal instability which was genuinely not captured by ECMWF PBLH model (Amiridis et al., 2010).

3.6 Vertical distribution of smoke AOD

The seasonally averaged BL and FT CALIOP smoke AOD over the upper IGP is depicted in Fig. 7, including vertical distribution of smoke AOD with reference to altitude. Throughout the year, smoke AOD was found to unevenly distribute against PBLH while the deviation between BL and FT smoke AOD enhanced particularly at night. Such observation however, may slightly influence by low sensitivity of CALIOP sensor in detecting low aerosol extinction especially at high altitude and in the FT.

On annual basis, daytime smoke AOD over the upper IGP was 1.42, 64% of which present within the free troposphere (FT). In contrast, nighttime smoke AOD was comparatively high (1.56), distributed primarily within the FT (84%) compared to the BL (16%). Beside these, irrespective of seasons, approximately 30 to 50% (50-80%) of smoke AOD remained within the first 1 (2) km of the lower atmosphere, clearly establishing the primary emissions from the local pollution sources.

Strong seasonality in smoke AOD partitioning between BL and FT was also noted likely due to the variation in emission sources, existing meteorology and aerosol transport. Likewise, 29% of daytime smoke AOD remained within the BL during DJF, while the fraction increased considerably in MAM (44%), possibly due to the corresponding increase in PBLH. The distinction between BL and FT smoke AOD was maximum during DJF, having 10% (nighttime) to 29% (daytime) smoke AOD within the BL compared to 70-90% of smoke AOD at FT. A reasonable explanation to such observation may be very low PBLH (465 m) during DJF which restrict vertical transport of smoke aerosols.

Partition of smoke AOD in JJAS (mean: 1.57) and ON (mean: 1.78) remained relatively stable compared to other seasons. Approximately 64% of daytime CALIOP smoke AOD was at FT and the fraction (82%) increased slightly during night. Both during JJAS and ON, smoke AOD at BL was slightly high during daytime (0.52-0.58; 34-36% of total smoke AOD) compared to nighttime (0.31-0.37; 18-20%). However, irrespective of day and night, almost 50% (66-80%) of smoke AOD during ON remained within the lowest 1 km (<2 km) of the atmosphere. During MAM, daytime CALIOP smoke AOD (1.29) partitioned almost equally within the FT (56%) and BL (44%), mainly due to the convective mixing of aerosols influenced by high PBLH (980 m). However, smoke aerosol was found to drift towards FT during night with 86% (1.14) smoke AOD prevail above PBLH compared to 14% at BL (0.18). Typical signature of nighttime smoke AOD during MAM was aerosol accumulation at 4 to 6 km height, contributing almost 34% of smoke AOD. As hypothesized, this may typically be the signature of transboundary aerosols transported from western dry regions by prevailing westerly.

It should be noted that, although we have reported to have higher fraction (Daytime: >56%; nighttime: >80%) of smoke AOD existing at free troposphere over the upper IGP, this was mainly partitioned against the prevailing PBLH that varied considerably, from 464 m (DJF) to 980 m (MAM). In contrast, approximately 30 to 50% (50-80%) of smoke AOD was retrieved within the lower 1 (<2) km of atmosphere throughout the year. This possibly indicate the persistence of smoke aerosols in close proximity to the surface which essentially deserves more attention in aerosol/-climate model, as this host potential to influence thermal/-oxidative balance of atmosphere, affecting human health beside regulating cloud formation processes.

Summary and conclusions

Vertical distribution of smoke aerosols against planetary boundary layer and average injection height of smoke aerosols was explored over the upper Indo-Gangetic Plain using space borne CALIOP attenuated backscatter lidar profile, between 2008 and 2017. Relative dominance of smoke aerosols over the entire South Asia was initially explored considering multiple satellite retrieved aerosol optical properties as a proxy for existing aerosol type and loading. Highly absorbing smoke aerosols were found to prevalent throughout the year, more abundantly between October and February months.

Throughout the year, near surface total aerosol extinction was >0.1 km^{-1} with highest extinction evident particularly at the surface, before decreasing with increasing height, indicating primary contribution of the local emission sources. On an average, the height of smoke aerosol extinction was 1.5 times lower to the total aerosols, and the difference increased particularly during MAM and JJAS when PBLH was at maximum. Near the surface the contribution of smoke extinction varied within a range of 2 to 50%, with highest contribution noted during DJF (~50%) and the lowest in MAM and JJAS (~2-5%). Diurnal variation in smoke aerosol extinction was both in terms of smoke height and intensity which reaffirm the influence of boundary layer in modulating vertical mixing of aerosols.

Smoke injection height during two extreme biomass burning seasons (AM and ON) were investigated. Average smoke injection heights for rice (ON) and wheat (AM) residue burning periods were 0.71 and 2.34 km, respectively. A significant positive association between injection height and boundary layer was also noted for both the cases. Smoke aerosols from wheat residue burning were found mostly to inject above the PBLH directly at free troposphere in contrast to the rice residue burning emissions which mostly remain confined under the boundary layer.

Vertical distribution of smoke AOD between the boundary layer (BL) and the free troposphere (FT) was also explored. On an annual basis, CALIOP nighttime smoke AOD (1.56) was higher compared to daytime (0.91), among which BL contributed almost 36% (16%) of smoke AOD during daytime (nighttime). Clearly the contribution of FT was higher compared to BL, and the distinction increased particularly in night (for all the seasons). Relative contribution of BL AOD to total smoke AOD reduced considerably during night (10-20%) compared to daytime (29-44%), referring efficient transport of smoke particles to the FT. We also partitioned existing smoke AOD for each km vertically above the surface. This however, indicate that despite of accounting 64-84% of smoke AOD above the PBLH, the major fraction of smoke AOD remained within the first 2-3 km above the surface. This remain one of the important conclusions from this experiment that after emission, smoke aerosols possibly transport efficiently above the PBLH at FT, thereby practically

reducing the level of human exposure; but it continues to prevail <3 km of the lower atmosphere thereby, have certain implications to regional climate. These evidences in uneven smoke aerosol portioning over the upper IGP may be crucial for regional climate/-air quality modelling to reduce uncertainties for computing radiative forcing, aerosol transport, aerosol-cloud interaction and in establishing aerosol-health relation over the region.

Data availability

MODIS data are available at Atmosphere Archive & Distribution System (LAADS) at https://ladsweb.nascom.nasa.gov. Aura-OMI data are available at Mirador-NASA Goddard Earth Sciences Data and Information Center (GES DISC) (https://mirador.gsfc.nasa.gov). CALIPSO data are available at NASA Atmospheric Science Data Center (https://eosweb.larc.nasa.gov). PBLH was retrieved from ERA-Interim Archive available at ECMWF website (https://ecmwf.int/en/). Modis Fire products are obtained from Fire Information for Resource Management System (FIRMS) (https://firms.modaps.eosdis.nasa.gov). All datasets were last accessed on April 2019.

Author Contributions

KSV and TB designed the research; KSV, AM and TB experimented, analyzed and interpreted the result. TB, AM, MSH, RKM and TL drafted the manuscript.

Competing interests. Authors declare that they have no conflict of interest.

Acknowledgements

The research is funded by SERB, Department of Science and Technology (DST), Government of India under ASEAN- India Collaborative R&D Scheme funded by ASEAN- India S&T Development Fund (CRD/2018/000011). TB acknowledges the financial support from University Grants Commission (UGC, 6-11/2018) and DB acknowledges Israel Science Foundation (ISF, 0472714) under UGC-ISF bilateral project; AM acknowledges the Jawaharlal Nehru Scholarship from Jawaharlal Nehru Memorial Fund (JNMF); MSH acknowledges the NASA Post-Doctoral Fellowship administered by USRA and RKM acknowledges the fund received from DST under Climate Change Programme (DST/CCP/CoE/80/2017 G).

References

1. Altaratz, O., Bar-Or, R. Z., Wollner, U., & Koren, I. (2013). Relative humidity and its effect on aerosol optical depth in the vicinity of convective clouds. *Environ. Res. Let.*, 8(3), 034025.

2. Amiridis, V., Giannakaki, E., Balis, D. S., Gerasopoulos, E., Pytharoulis, I., Zanis, P., Kazadzis, S., Melas, D., and Zerefos, C. (2010). Smoke injection heights from agricultural burning in Eastern Europe as seen by CALIPSO, *Atmos. Chem. Phys*., 10, 11567-11576.

3. Andreae MO, Gelencsér A (2006) Black carbon or brown carbon? The nature of light absorbing carbonaceous aerosols. *Atmos Chem Phys* 6:3131–3148.

4. Banerjee, T., Kumar, M., Mall, R. K., & Singh, R. S. (2017). Airing 'clean air' in clean India mission. *Environ.* Sci. and Poll. Res., 24(7), 6399-6413.

5. Babu SS, Moorthy KK, Manchanda RK, Sinha PR, Satheesh SK, Vajja DP, et al. (2011). Free tropospheric black carbon aerosol measurements using high altitude balloon: do BC layers build "their own homes" up in the atmosphere? *Geophys. Res. Lett.* 38, L08803, doi:10.1029/2011GL046654.

6. Bilal, M., Nichol, J.E. and Chan, P.W., 2014. Validation and accuracy assessment of a Simplified Aerosol Retrieval Algorithm (SARA) over Beijing under low and high aerosol loadings and dust storms. Remote sensing of environment, 153, pp.50-60.

7. Bilal, M. and Nichol, J.E., 2015. Evaluation of MODIS aerosol retrieval algorithms over the Beijing-Tianjin-Hebei region during low to very high pollution events. *J. Geophys. Res.-Atmos*, 120(15), pp.7941-7957.

8. Bond TC, Doherty SJ, Fahey DW, Forster PM, Berntsen T, De Angelo BJ, et al. (2013). Bounding the role of black carbon in the climate system: a scientific assessment*, J Geophys. Res*., 118:5380–5552.

9. Bourgeois, Q., Ekman, A. M. L., Renard, J.-B., Krejci, R., Devasthale, A., Bender, F. A.-M., Riipinen, I., Berthet, G., and Tackett, J. L. (2018). How much of the global aerosol optical depth is found in the boundary layer and free troposphere?, *Atmos. Chem. Phys*., 18, 7709-7720.

10. Chowdhury, S., S. Dey, L. Di Girolamo, K. R. Smith, A. Pillarisetti and A. Lyapustin, 2019. Tracking ambient PM2.5 build-up in Delhi national capital region during the dry season over 15 years using a high-resolution (1 km) satellite aerosol dataset, Atmospheric Environment, 204, 142-150.

11. Chen, Y., Li, Q., Randerson, J. T., Lyons, E. A., Kahn, R. A., Nelson, D. L., and Diner, D. J. (2009). The sensitivity of CO and aerosol transport to the temporal and vertical distribution of North American boreal fire emissions, *Atmos. Chem. Phys.,* 9, 6559–6580.

12. Dey, S., & Di Girolamo, L. (2011). A decade of change in aerosol properties over the Indian subcontinent. *Geophys Res. Lett.*, *38*(14).

13. Dey, S., Tripathi, S. N., Singh, R. P., & Holben, B. N. (2004). Influence of dust storms on the aerosol optical properties over the Indo-Gangetic basin. *J. Geophys. Res.-Atmos., 109*(D20).

14. Eck, T. F., Holben, B. N., Reid, J. S., Mukelabai, M. M., Piketh, S. J., Torres, O., Jethva, H. T., Hyer, E. J., Ward, D. E., Dubovik, O., Sinyuk, A., Schafer, J. S., Giles, D. M., Sorokin, M., Smirnov, A., and Slutsker, I. (2013). A seasonal trend of single scattering albedo in southern African biomass-burning particles: implications for satellite products and estimates of emissions for the world's largest biomass-burning source, *J. Geophys. Res.-Atmos*., 118, 6414–6432.

15. Feingold, G., Remer, L. A., Ramaprasad, J., and Kaufman, Y. J. (2001). Analysis of smoke impact on clouds in Brazilian biomass burning regions: An extension of Twomey's approach, *J. Geophys. Res.*, 106, 22907–22922.

16. Freitas, S. R., Longo, K. M., Chatfield, R., Latham, D., Silva Dias, M. A. F., Andreae, M. O., Prins, E., Santos, J. C., Gielow, R., and Carvalho Jr., J. A. (2007). Including the sub-grid scale plume rise of vegetation fires in low resolution atmospheric transport models, *Atmos. Chem. Phys*., 7, 3385–3398.

17. Gautam, R., Hsu, N. C., Tsay, S. C., Lau, K. M., Holben, B., Bell, S. et al. & Payra, S. (2011). Accumulation of aerosols over the Indo-Gangetic plains and southern slopes of the Himalayas: distribution, properties and radiative effects during the 2009 pre-monsoon season. *Atmos. Chem. and Phys*, 11(24), 12841-12863.

18. Gautam, R., Hsu, N.C. and Lau, K.M., (2010). Premonsoon aerosol characterization and radiative effects over the Indo-Gangetic Plains: Implications for regional climate warming. *J. Geophys. Res.*, 115(D17).

19. Giglio, L., Descloitres, J., Justice, C.O., Kaufman, Y., 2003. An enhanced contextual fire detection algorithm for MODIS. *Remote Sens. Environ*. 87, 273-282.

20. Guan, H., Esswein, R., Lopez, J., Bergstrom, R., Warnock, A., Follette-Cook, M., Fromm, M., and Iraci, L. T. (2010). A multi-decadal history of biomass burning plume heights identified using aerosol index measurements*, Atmos. Chem. Phys*., 10, 6461-6469.

21. Gupta, P., Remer, L. A., Levy, R. C., & Mattoo, S. (2018). Validation of MODIS 3 km land aerosol optical depth from NASA's EOS Terra and Aqua missions. *Atmos. Measure. Tech.*, 11(5), 3145-3159.

22. Ho, H.C., Wong, M.S., Yang, L., Shi, W., Yang, J., Bilal, M. and Chan, T.C., 2018. Spatiotemporal influence of temperature, air quality, and urban environment on cause-specific mortality during hazy days. *Environment international*, *112*, pp.10-22.

23. Janssen, N. A., Hoek, G., Simic-Lawson, M., Fischer, P., Van Bree, L., Ten Brink, H., Keuken, M., Atkinson, R. W., Anderson, R., Brunekreef, B., and Cassee, F. R. (2011). Black carbon as an additional indicator of the adverse health effects of airborne particles compared with PM10 and PM2.5. *Environ. Health Perspect.*, 119(12), 1691-1699.

24. Jethva, H., S. K. Satheesh, and J. Srinivasan (2005), Seasonal variability of aerosols over the Indo-Gangetic basin, J. Geophys. Res., 110, D21204, doi:10.1029/2005JD005938

25. Jethva, H., Chand, D., Torres, O., Gupta, P., Lyapustin, A., & Patadia, F. (2018). Agricultural burning and air quality over northern India: a synergistic analysis using NASA's A-train satellite data and ground measurements. *Aerosol and Air Quality Research*, 18, 1756-1773.

26. Jethva, H., Torres, O., and Ahn, C. 2018. A 12-year long global record of optical depth of absorbing aerosols above the clouds derived from the OMI/OMACA algorithm, Atmos. Meas. Tech., 11, 5837-5864.

27. Jethva, H., Torres, O., Waquet, F., Chand, D., and Hu, Y. (2014), How do A-train sensors intercompare in the retrieval of above-cloud aerosol optical depth? A case study-based assessment, Geophys. Res. Lett., 41, 186– 192.

28. Kahn, R. A., Chen, Y., Nelson, D. L., Leung, F. Y., Li, Q., Diner, D. J., & Logan, J. A. (2008). Wildfire smoke injection heights: Two perspectives from space. *Geophys. Res. Lett.*, 35(4).

29. Kaskaoutis, D. G., Kumar, S., Sharma, D., Singh, R. P., Kharol, S. K., Sharma, M., Singh, A. K., Singh, S., Singh, A., and Singh, D. (2014). Effects of crop residue burning on aerosol properties, plume characteristics, and long-range transport over northern India, *J. Geophys. Res.-Atmos.,* 119, 5424–5444.

30. Meyer, K., Platnick, S., and Zhang, Z.: Simultaneously inferring above-cloud absorbing aerosol optical thickness and underlying liquid phase cloud optical and microphysical properties using MODIS, J. Geophys. Res.-Atmos., 120, 5524–5547, https://doi.org/10.1002/2015JD023128, 2015

31. Kim, M.-H., Omar, A. H., Tackett, J. L., Vaughan, M. A., Winker, D. M., Trepte, C. R., Hu, Y., Liu, Z., Poole, L. R., Pitts, M. C., Kar, J., and Magill, B. E. (2018). The CALIPSO version 4 automated aerosol classification and lidar ratio selection algorithm, Atmos. Meas. Tech., 11, 6107-6135.

32. Kim, M.H., Kim, S.W., Yoon, S.C. and Omar, A.H., 2013. Comparison of aerosol optical depth between CALIOP and MODIS-Aqua for CALIOP aerosol subtypes over the ocean. *Journal of Geophysical Research: Atmospheres*, *118*(23), pp.13-241.

33. Kirchstetter, T. W., T. Novakov, and P. V. Hobbs (2004), Evidence that the spectral dependence of light absorption by aerosols is affected by organic carbon, J. Geophys. Res., 109, D21208, doi:10.1029/2004JD004999

34. Koffi, B., Schulz, M., Bréon, F.-M., Dentener, F., Steensen, B. M., Griesfeller, J.,Winker, D., Balkanski, Y., Bauer, S., Bellouin, N., Berntsen, T., Bian, H., Chin, M., Diehl, T., Easter, R., Ghan, S., Hauglustaine, D. A., Iversen, T., Kirkevåg, A., Liu, X., Lohmann, U., Myhre, G., Rasch, P., Seland, Ø., Skeie, R. B., Steenrod, S. D., Stier, P., Tackett, J., Takemura, T., Tsigaridis, K., Vuolo, M. R., Yoon, J., and Zhang, K. (2016). Evaluation of the aerosol vertical distribution in global aerosol models through comparison against CALIOP measurements: AeroCom phase II results, *J. Geophys. Res*., 121, 7254–7283.

35. Koren I, Kaufman YJ, Remer LA, Martins JV. (2004). Measurement of the effect of Amazon smoke on inhibition of cloud formation. *Science*, 303, 1342–1345.

36. Krotkov, N. A., Lamsal, L. N., Celarier, E. A., Swartz, W. H., Marchenko, S. V., Bucsela, E. J., Chan, K. L., Wenig, M., and Zara, M. (2017). The version 3 OMI NO_2 standard product, *Atmos. Meas. Tech*., 10, 3133-3149.

37. Kumar, M., Parmar, K.S., Kumar, D.B., Mhawish, A., Broday, D.M., Mall, R.K., and Banerjee, T. (2018a). Long-term aerosol climatology over Indo-Gangetic Plain: Trend, prediction and potential source fields, Atmos. Environ., 180, 37-50.

38. Kumar, A., Singh, N. and Solanki, R., (2018b). Evaluation and utilization of MODIS and CALIPSO aerosol retrievals over a complex terrain in Himalaya. *Remote sensing of environment*, *206*, pp.139-155.

39. Kumar M, Singh RK, Murari V, Singh AK, Singh RS and Banerjee T. 2016. Fireworks induced particle pollution: A spatio-temporal analysis. *Atmos Res*, 180: 78–91.

40. Labonne, M., Breon, F.-M., and Chevallier, F. (2007). Injection height of biomass burning aerosols as seen from a spaceborne lidar, Geophys. Res. Lett., 34, L11806.

41. Lee, W-S. and Kim, M-K. (2010). Effects of radiative forcing by black carbon aerosol on spring rainfall decrease over Southeast Asia. *Atmos. Environ.* 44 (2010) 3739-3744.

42. Levelt, P.F., Hilsenrath, E., Leppelmeier, G.W., van den Ooord, G.H.J., Bhartia, P.K., Taminnen, J., de Haan, J.F., Veefkind, J.P., 2006. Science objectives of the Ozone monitoring Instrument. *IEEE Trans. Geosci. Remote Sens*. 44 (5), 1093-1101.

43. Levy, R.C., Mattoo, S., Munchak, L.A., Remer, L.A., Sayer, A.M., Patadia, F. and Hsu, N.C., 2013. The Collection 6 MODIS aerosol products over land and ocean. *Atmos. Measure. Tech*., 6(11), p.2989.

44. Lyapustin, A.I., Wang, Y., Laszlo, I., Hilker, T., Hall, F.G., Sellers, P.J., Tucker, C.J., Korkin, S.V., (2012). Multi-angle implementation of atmospheric correction for MODIS (MAIAC): 3. Atmospheric correction. Remote Sens. Environ. 127, 385–393.

45. Lyapustin, A., Wang, Y., Korkin, S., and Huang, D. (2018). MODIS Collection 6 MAIAC algorithm, Atmos. Meas. Tech., 11, 5741-5765.

46. Menut, L., Flamant, C., Pelon, J., and Flamant, P. (1999). Urban boundary layer height determination from lidar measurements over the Paris area, *Appl. Opt*., 38, 945–954.

47. Mhawish A, Banerjee T, Sorek-Hamer M, Lyapustin AI, Broday DM, Chatfield R. (2019). Comparison and evaluation of MODIS Multi-Angle Implementation of Atmospheric Correction (MAIAC) aerosol product over South Asia. *Remote Sens. Environ.* 224: 12–28.

48. Mhawish, A., Banerjee, T., Broday, D.M., Misra, A. and Tripathi, S.N., 2017. Evaluation of MODIS Collection 6 aerosol retrieval algorithms over Indo-Gangetic Plain: Implications of aerosols types and mass loading. *Remote Sensing of Environment*, 201, pp.297-313.

49. Mims, S. R., Kahn, R. A., Moroney, C. M., Gaitley, B. J., Nelson, D. L., and Garay, M. J. (2010). MISR Stereo Heights of Grassland Fire Smoke Plumes in Australia, IEEE Trans. Geosci. Remote Sens., 48, 25–35, No. 1.

50. Penning de Vries, M. J. M., Beirle, S., Hörmann, C., Kaiser, J. W., Stammes, P., Tilstra, L. G., Tuinder, O. N. E., and Wagner, T. (2015). A global aerosol classification algorithm incorporating multiple satellite data sets of aerosol and trace gas abundances, *Atmos. Chem. Phys*., 15, 10597-10618.

51. Penning de Vries, M. J. M., Beirle, S., Hörmann, C., Kaiser, J. W., Stammes, P., Tilstra, L. G., & Wagner, T. (2015). A global aerosol classification algorithm incorporating multiple satellite data sets of aerosol and trace gas abundances. *Atmos. Chem. and Phys., 15*(18), 10597-10618.

52. Rajput, P., and Sarin, M.M. (2014). Polar and non-polar organic aerosols from large-scale agricultural-waste burning emissions in Northern India: implications to organic mass-to-organic carbon ratio, *Chemosphere*, 103, 74-79.

53. Satheesh, S. K., Krishna Moorthy, K., Suresh Babu, S., Vinoj, V., Nair, V. S., Naseema Beegum, S., & Kunhikrishnan, P. K. (2009). Vertical structure and horizontal gradients of aerosol extinction coefficients over coastal India inferred from airborne lidar measurements during the Integrated Campaign for Aerosol, Gases and Radiation Budget (ICARB) field campaign. *J. Geophys. Res.-Atmos*, 114(D5).

54. Sayer, A. M., Hsu, N. C., Lee, J., Kim, W. V., & Dutcher, S. T. Validation, stability, and consistency of MODIS Collection 6.1 and VIIRS Version 1 Deep Blue aerosol data over land. *J. Geophys. Res. Atmos* 124(8): 4658-4688.

55. Sayer, A.M., Munchak, L.A., Hsu, N.C., Levy, R.C., Bettenhausen, C., Jeong, M. (2015). MODIS Collection 6 aerosol products: comparison between Aqua's e-deep blue, dark target, and "merged" data sets, and usage recommendations. *J. Geophys. Res. Atmos*., 119 (24), pp. 13,965-13,989.

56. Sayer, A.M., Munchak, L.A., Hsu, N.C., Levy, R.C., Bettenhausen, C. and Jeong, M.J., 2014. MODIS Collection 6 aerosol products: Comparison between Aqua's e-Deep Blue, Dark Target, and "merged" data sets, and usage recommendations. *J. Geophys. Res.-Atmos*, 119(24).

57. Sen, A., Abdelmaksoud, A. S., Ahammed, Y. N., Banerjee, T., Bhat, M. A., Chatterjee, A. ... & Gadi, R. (2017). Variations in particulate matter over Indo-Gangetic Plains and Indo-Himalayan Range during four field campaigns in winter monsoon and summer monsoon: Role of pollution pathways. *Atmos. Environ*., 154, 200-224.

58. Sharma, G., Sinha, B., Pallavi, Hakkim, H., Chandra, B.P., Kumar, A. and Sinha, V., (2019). Gridded emissions of CO, NOx, SO2, CO2, NH3, HCl, CH4, PM2.5, PM10, BC and NMVOC from open municipal waste burning in India. *Environmental Science & Technology*. DOI: 10.1021/acs.est.8b07076.

59. Singh N, Banerjee T, Raju MP, Deboudt K, Sorek-Hamer M, Singh RS, Mall RK, (2018). Aerosol chemistry, transport and climatic implications during extreme biomass burning emissions over Indo-Gangetic Plain. *Atmos. Chem. and Phys.* 18, 14197-14215.

60. Singh N, Mhawish A, Deboudt K, Singh RS and Banerjee T. 2017b. Organic aerosols over Indo-Gangetic Plain: Sources, distributions and climatic implications. *Atmos. Environ*. 157: 59-74.

61. Singh N, Murari V, Kumar M, Barman SC and Banerjee T. 2017a. Fine particulates over South Asia: Review and meta-analysis of PM2.5 source apportionment through receptor model. Environmental Pollution. 223: 121-136.

62. Singh, A. and Dey, S., (2012). Influence of aerosol composition on visibility in megacity Delhi, *Atmos. Environ.*, 62, 367-373.

63. Stull, R. B. (1988). An introduction to boundary-layer meteorology, Kluwer Academic Publishers, Springer, the Netherlands.

64. Torres, O., A. Tanskanen, B. Veihelmann, C. Ahn, R. Braak, P. K. Bhartia, P. Veefkind, and P. Levelt (2007), Aerosols and surface UV products from Ozone Monitoring Instrument observations: An overview, *J. Geophys. Res*., 112, D24S47.

65. Torres, O., Ahn, C., and Chen, Z. (2013). Improvements to the OMI near-UV aerosol algorithm using A-train CALIOP and AIRS observations, *Atmos. Meas. Tech*., 6, 3257-3270.

66. Toth, T. D., Zhang, J., Campbell, J. R., Reid, J. S., and Vaughan, M. A. (2016). Temporal variability of aerosol optical thickness vertical distribution observed from CALIOP, *J. Geophys. Res.,* 121, 9117–9139.

67. Toth, T. D., Campbell, J. R., Reid, J. S., Tackett, J. L., Vaughan, M. A., Zhang, J., and Marquis, J. W. 2018. Minimum aerosol layer detection sensitivities and their subsequent impacts on aerosol optical thickness retrievals in CALIPSO level 2 data products, Atmos. Meas. Tech., 11, 499–514.

68. Vadrevu, K. P., Ellicott, E., Badarinath, K. V. S., & Vermote, E. (2011). MODIS derived fire characteristics and aerosol optical depth variations during the agricultural residue burning season, north India. *Environ. Poll.*, 159(6), 1560-1569.

69. Val Martin, M., Logan, J. A., Kahn, R. A., Leung, F.-Y., Nelson, D. L., and Diner, D. J. (2010). Smoke injection heights from fires in North America: analysis of 5 years of satellite observations, *Atmos. Chem. Phys*., 10, 1491–1510.

70. Veefkind, J. P., Aben, I., McMullan, K., Förster, H., de Vries, J., Otter, G., Claas, J., Eskes, H. J., de Haan, J. F., Kleipool, Q., van Weele, M., Hasekamp, O., Hoogeveen, R., Landgraf, J., Snel, R., Tol, P., Ingmann, P., Voors, R., Kruizinga, B., Vink, R., Visser, H., and Levelt, P. F. (2012). TROPOMI on the ESA Sentinel-5 Precursor: a GMES mission for global observations of the atmospheric composition for climate, air quality and ozone layer applications, *Remote Sens. Environ*., 120, 70–83.

71. Vermote, E.F. and Kotchenova, S., 2008. Atmospheric correction for the monitoring of land surfaces. Journal of Geophysical Research: Atmospheres, 113(D23).

720 72. Von Engeln, A. and Teixeira, J. (2013). A Planetary Boundary Layer Height Climatology Derived from
721 ECMWF Reanalysis Data, *J. Climate*, 26, 6575–6590.

722 73. Wang, C., (2004). A modeling study on the climate impacts of black carbon aerosols. *J. Geophys. Res.,* 109,
723 D03106.

724 74. Wei, J., Li, Z., Peng, Y., & Sun, L. (2019). MODIS Collection 6.1 aerosol optical depth products over land and
725 ocean: validation and comparison. *Atmos. Environ.*, 201, 428-440.

726 75. Winker, D. M., Vaughan, M. A., Omar, A., Hu, Y., Powell, K. A., Liu, Z., Hunt, W. H., and Young, S. A. (2009).
727 Overview of the CALIPSO Mission and CALIOP Data Processing Algorithms, *J. Atmos. Ocean. Tech*., 26,
728 2310–2323.

729 76. Young, A. and Vaughan, M. A. (2009). The Retrieval of Profiles of Particulate Extinction from Cloud-Aerosol
730 Lidar Infrared Pathfinder Satellite Observations (CALIPSO) Data: Algorithm Description, *J. Atmos. Ocean.*
731 *Tech*., 26, 1105–1119.

732 77. Zhang, Z.*, K. Meyer, H. Yu, S. Platnick, P. Colarco, Z. Liu, and L. Oreopoulos (2016), Shortwave direct
733 radiative effects of above-cloud aerosols over global oceans derived from 8 years of CALIOP and MODIS
734 observations, ACP, 16(5), 2877–2900, doi:10.5194/acpd-15-26357-2015.

735 78. Zhang, L., Henze, D. K., Grell, G. A., Carmichael, G. R., Bousserez, N., Zhang, Q., Torres, O., Ahn, C., Lu, Z.,
736 Cao, J., and Mao, Y. (2015). Constraining black carbon aerosol over Asia using OMI aerosol absorption
737 optical depth and the adjoint of GEOS-Chem, *Atmos. Chem. Phys*., 15, 10281-10308.

738 79. Zhang, L., Henze, D. K., Grell, G. A., Torres, O., Jethva, H., & Lamsal, L. N. (2017). What factors control the
739 trend of increasing AAOD over the United States in the last decade?. *J. Geophys. Res.-Atmos*, 122(3), 1797-
740 1810.

741

742 **List of Figures**

756

757

758

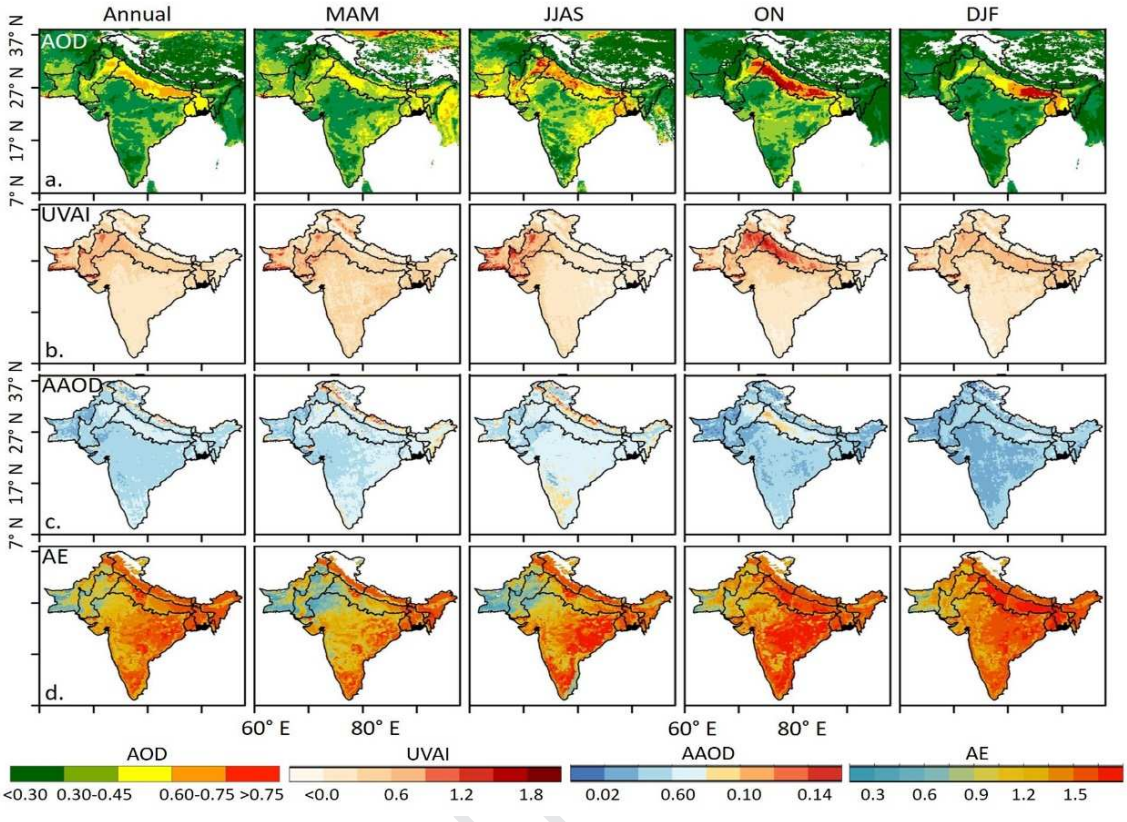

759

760 Fig. 1. Spatiotemporal variations of aerosol optical properties over South Asia, 2008-2017.

761

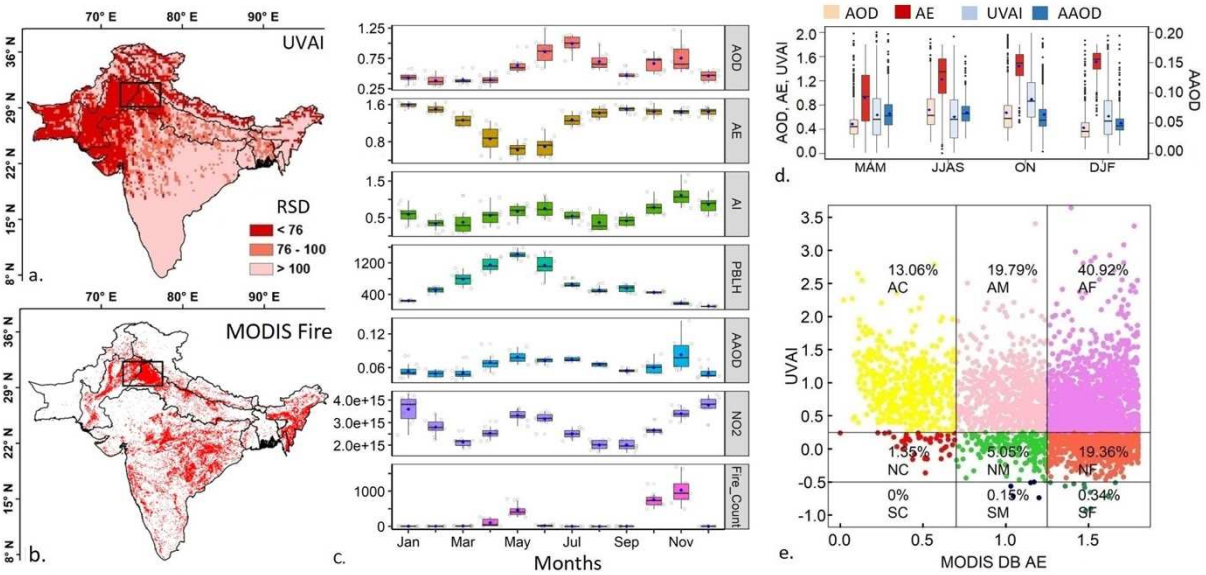

Fig. 2. Spatiotemporal variations of (a) the relative standard deviation of the UVAI, and (b) the MODIS fire count; (c) monthly variations of AOD, AE, AI, PBLH (m), AAOD, NO_2 (molecules cm^{-2}), and fire count in the box specified in (a); (d) seasonal distributions of AOD, AE, UVAI, and AAOD over the box specified in (a); and (e) speciation of aerosol types based on aerosol absorption (UVAI) and size (AE).

Note. Fig. 2a and 2b represent annual mean based on decadal dataset while Fig. 2c represent monthly means of individual parameter based on 10-years dataset (2008-2017). The box indicated in the upper left panel was selected for CALISPO retrieval based on higher abundance of smoke aerosols. Aerosol types color-coded according to size and absorption. The first character in aerosol types represents the optical properties A: Absorbing, N: Neutral, and S: Scattering, and the second character represents size F: Fine, M: Mixed and C: coarse. For example, AF represent Absorbing Fine aerosol type.

777

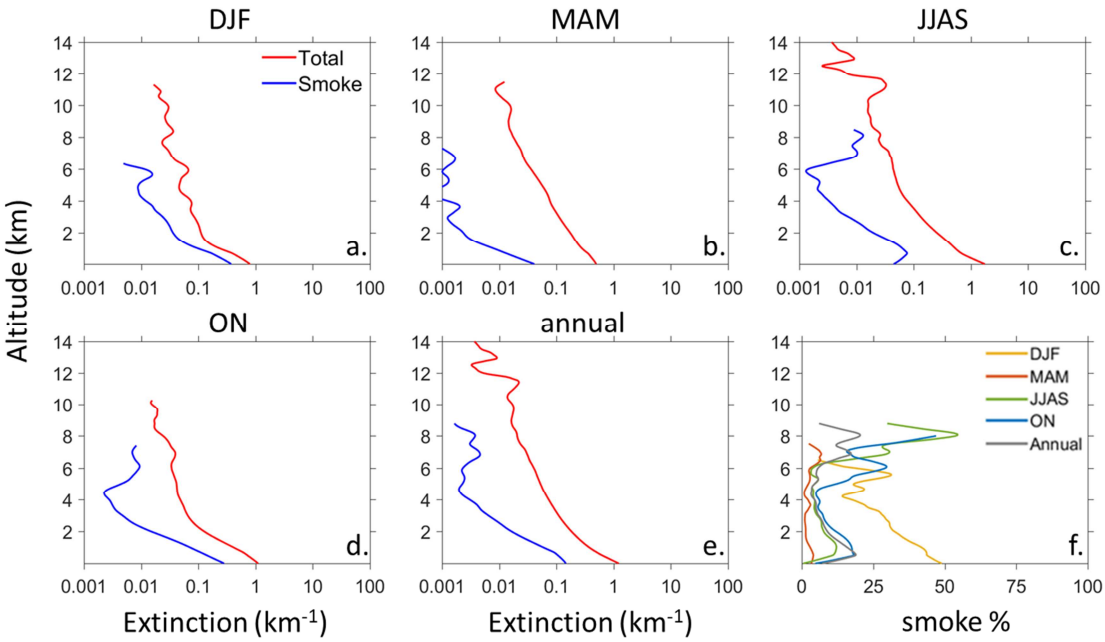

778
779

780 Fig. 3. Vertical distribution of smoke aerosols over upper IGP (a-d) seasonal variations, (e)
781 annual profile and (f) smoke contribution to total aerosol extinction (%).

782

783

784

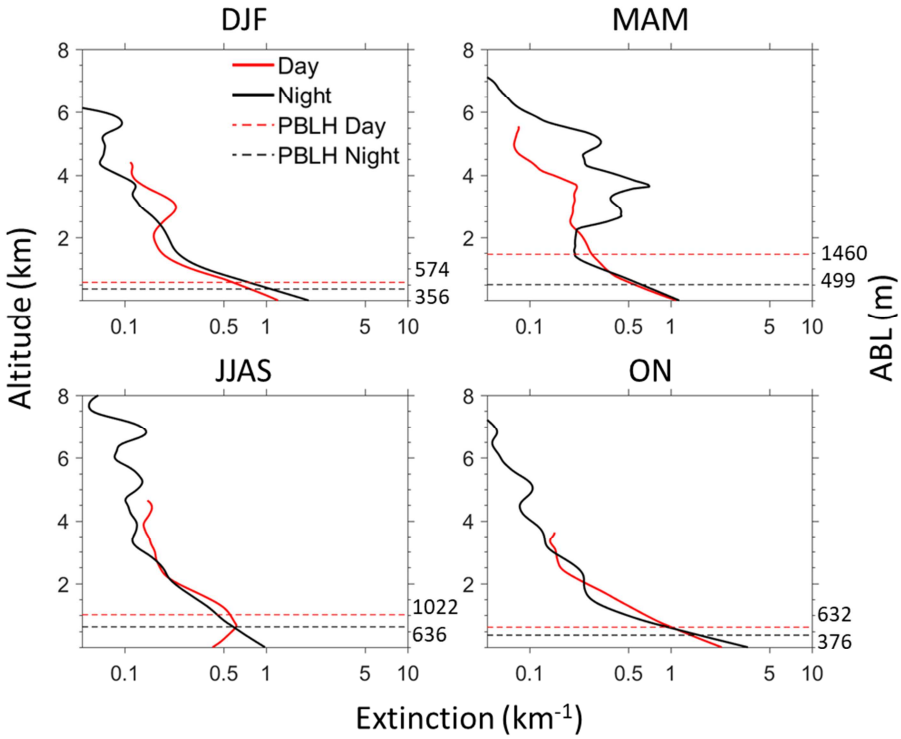

785

786 Fig. 4. Diurnal variations of the mean smoke extinction relative to boundary layer height.

787

788

789

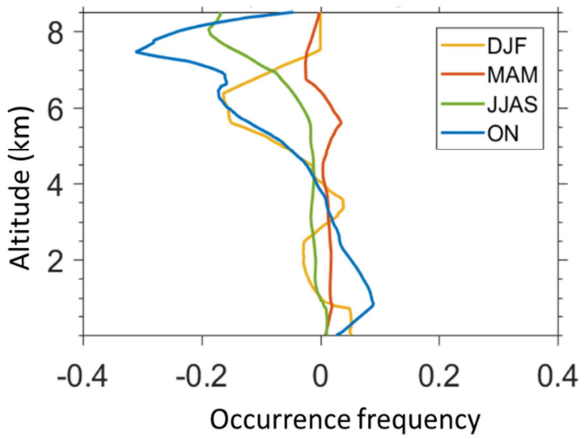

790

791 Fig. 5. Seasonal variation of smoke aerosols day-night occurrence frequency.

792

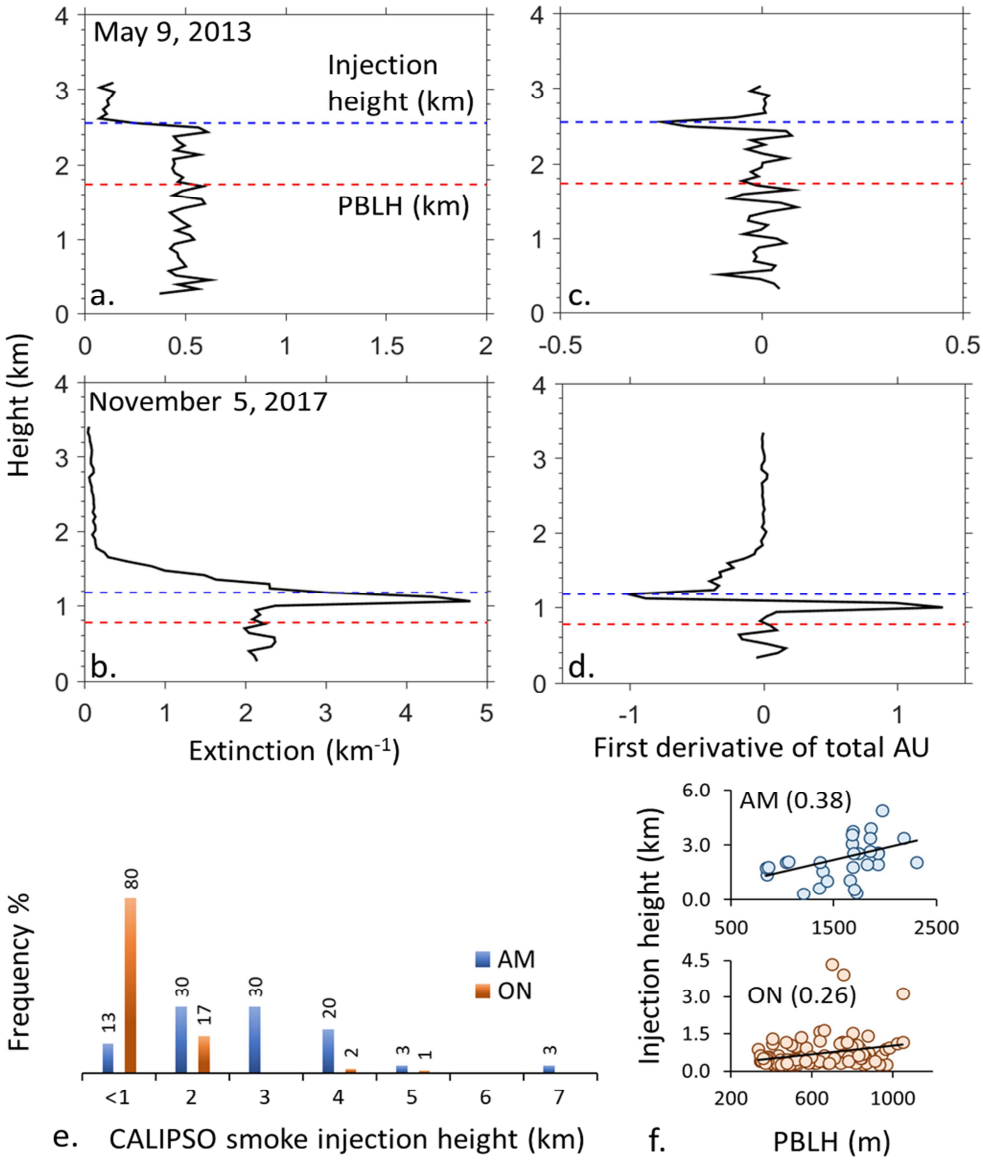

Fig. 6. Variation in smoke injection height against the PBLH during two intense biomass burning seasons, (a-b) Calispo attenuated backscatter at 532 nm and (c-d) the corresponding first derivate of the attenuated backscatter (AU) during typical rice and wheat residue burning period, (e) frequency distribution of smoke injection height and (f) comparison of smoke injection height against PBLH.

Note. Values in parenthesis in Fig.6f indicate correlation coefficient.

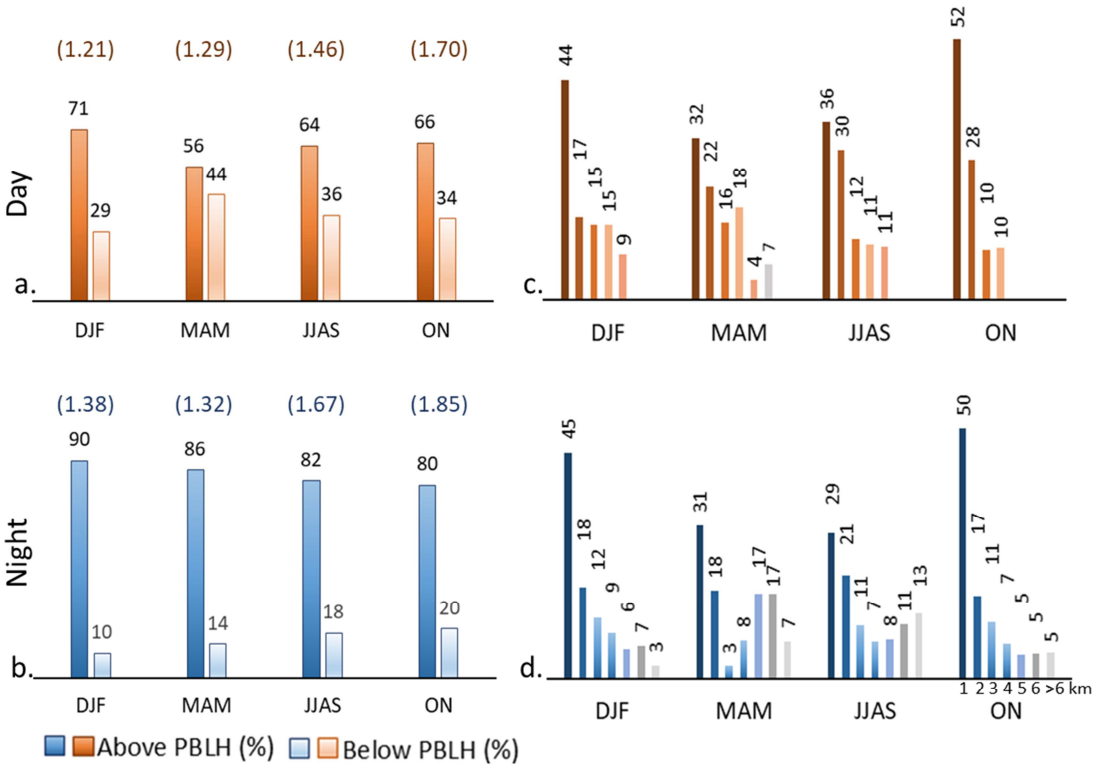

Fig. 7. Vertical distribution of smoke AOD over upper IGP, (a-b) diurnal variation against PBLH, and (c-d) relative percentage of smoke AOD in each km above the surface.

Note. Values in parenthesis indicate total smoke AOD.

Highlights

1. Across South Asia, smoke aerosols were most abundant over upper Indo-Gangetic Plain.
2. Relative abundance of smoke days' increases during October to February months.
3. Smoke injection height was higher in wheat compared to rice residue burning period.
4. Almost 74% of smoke AOD remain above the boundary layer at the free troposphere.
5. Overall, 50-80% of CALISPO smoke AOD remain very close (< 3 km) to the surface.